DASA-2665
3SR-513
DECEMBER 30, 1970

DETERMINATION OF TEST NEEDS FOR THE PRIME ARGUS PROGRAM

FINAL REPORT

G. D. ANDERSON

HEADQUARTERS
DEFENSE ATOMIC SUPPORT AGENCY
WASHINGTON, D. C.

SYSTEMS, SCIENCE AND SOFTWARE
LA JOLLA, CALIFORNIA 92037

CONTRACT NO. DASA 01-70-C-0122

Destroy this report when it is no longer needed. Do not return to sender.

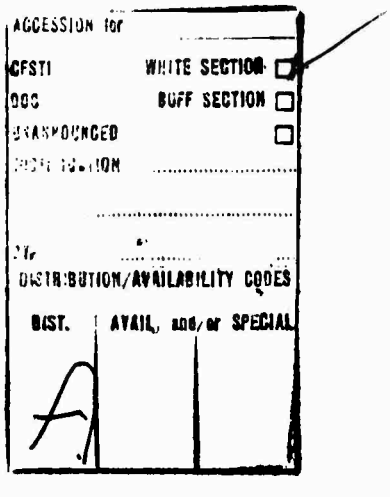

SYSTEMS, SCIENCE AND SOFTWARE

DASA 2665
3SR-513

DETERMINATION OF TEST NEEDS FOR THE PRIME ARGUS PROGRAM

FINAL REPORT

PRINCIPAL INVESTIGATOR: G.D. ANDERSON (714) 453-0060
PROJECT SCIENTIST: MR. C.B. McFARLAND, DASA

THIS WORK WAS SUPPORTED BY
THE ADVANCED RESEARCH PROJECTS AGENCY
UNDER ARPA ORDER NO. 1438, PROGRAM CODE 0F10

CONTRACT NO. DASA 01-70-C-0122
EFFECTIVE DATE OF CONTRACT: 1 JUNE 1970
CONTRACT COMPLETION DATE: 31 MARCH 1971 S^3 PROJECT 132

DECEMBER 30, 1970

P.O. BOX 1620, LA JOLLA, CALIFORNIA 92037, TELEPHONE (714) 453-0060

ACKNOWLEDGEMENTS

The author wishes to acknowledge Mr. Kenneth G. Hamilton for performing all the computer runs and Dr. T. David Riney and Mr. Carl R. Hastings for discussions on the equation of state.

CONTENTS

Acknowledgements. iii

List of Illustrations v

List of Tables. vi

Abstract. vii

1. INTRODUCTION. 1

2. EQUATION OF STATE MODEL AND CALCULATION METHOD. . . 3

2.1 Hydrodynamic Equation of State. 3
2.2 Material Strength 7
2.3 Method of Computation 9

3. SPHERICAL WAVE PROPAGATION IN TUFF. 11

3.1 Peak Stress 13
3.2 Arrival Times and Pulse Widths. 20
3.3 Displacement and Velocity 29

4. SUMMARY 33

References 35

LIST OF ILLUSTRATIONS

Figure		Page
1	Pressure vs distention ratio for a generalized porous material.	5
2	Pressure vs specific volume for a generalized porous material.	8
3	Attenuation of peak radial stress.	15
4	Radial stress-time profiles for Run 0D.	17
5	Radial stress-time profiles for Run 1C.	21
6	Radial stress-time profiles for Run 10A.	24
7	Radial stress-time profiles for Run 3C	27

LIST OF TABLES

Table		Page
I	Parameters used in Spherical Calculations	12
II	Peak Stress as a Function of Radius	14
III	Arrival Times and Pulse Widths as Functions of Radius	30
IV	Position and Velocity at t ∿ 75 μsec	31

ABSTRACT

A series of spherical one-dimensional computer code calculations was performed to assess the effects of mechanical material property parameters on wave propagation in dry porous and compacted tuff. Peak stress attenuation was found to be most sensitive to initial porosity. In compacted material peak stress attenuation was found to be more sensitive to the shear modulus than to the yield strength. Increasing hoop tensile stresses occurred with increasing yield strength. Introduction of a hoop tensile fracture criterion did not affect peak stress attenuation but did affect the radial displacement. Generally radial displacements of particles at the same initial radius from the source increased with increasing porosity. Shock wave arrival times at various distances from the source increased with increasing porosity.

I. INTRODUCTION

In order to satisfactorily predict stress wave propagation in the earth resulting from an underground explosion, it is necessary to know certain material properties of the earth which govern its response to dynamic loads. The present study was undertaken as a preliminary attempt to determine the relative importance of various mechanical material parameters on spherically symmetric wave propagation in a rock which may be porous. The problem studied consists of a spherical cavity in the rock with an initial radius of 5 cm. At time $t = 0$, a normal stress $\sigma(r_c,t)$ is applied to the interior surface of the cavity. A one-dimensional Lagrangian finite-difference computer code is used to compute the subsequent stress field in the rock. The radial stress, $\sigma_r(r, t)$, the tangential stress, $\sigma_\theta(r, t)$, and the hydrostatic pressure, $P(r, t)$, are calculated as functions of time along the paths of selected particles which are initially at 7.5, 10, 12.5, 25 and 30 cm from the center of the cavity. Although all problems were run using the above dimensions, scaling of the problems to different dimensions would not alter the relative importance of wave propagation on the various material property parameters considered. In addition to the stress field, particle displacements are also computed.

The mechanical material property parameters which are varied in this parameter study were chosen to be representative of dry Nevada Test Site (NTS) tuff. Inasmuch as this was a parameter study, no attempt was made to simulate specificially in detail any of the many NTS tuffs which exist in the field. The effect of moisture was not considered in this study.

The following sections describe the material property model, the computation technique and the results obtained from several computations in which the values of the mechanical parameters were varied.

2. EQUATION OF STATE MODEL AND CALCULATION METHOD

The equation of state model used to represent dry porous tuff in the present parameter study is the S^3 Porous EOS model.[1,2] This model includes a hydrostatic pressure-volume-energy (P-V-E) relationship which provides for irreversible void collapse plus deviatoric stresses to provide for shear strength. The P-V-E model is quite similar to that developed by Herrmann.[3]

2.1 HYDRODYNAMIC EQUATION OF STATE

The solid (void free) material is assumed to obey a Mie-Gruneisen equation of state

$$P = P_r + G\rho\left(E - E_r\right) \tag{1}$$

where P_r is some reference curve in the P-V plane, E_r is the specific internal energy along that curve, G is Gruneisen's ratio which is assumed constant, and $\rho = 1/V$ is the density of the solid material. The reference curve is frequently taken to be the principal Hugoniot curve of the solid material in the form

$$P_H(\rho) = A\eta + B\eta^2 + C\eta^3 \tag{2}$$

where $\eta = \rho/\rho_0 - 1$ and A, B, and C are constants. The specific internal energy along the Hugoniot is then given by

$$E_H = E_0 + \frac{1}{2} P_H \left(V_0 - V\right) \tag{3}$$

When dealing with a porous material a distension ratio, α, defined as

$$\alpha \equiv \frac{\rho_s(P, E)}{\rho_p(P, E)} \tag{4}$$

is introduced. Here ρ_s is the density of the void free material at a given value of pressure and internal energy and ρ_p is the density of the porous material at the same value of the pressure and internal energy. The compaction or crushup process of the porous material is then modeled through the parameter α. In general α could depend upon the deviatoric stresses in addition to the hydrostatic pressure and internal energy. The Mie-Gruneisen equation of state for the porous material is obtained by combining Eqs. (1), (2) and (4),

$$P = P_H(\alpha\rho_p) + G\,\alpha\,\rho_p(E - E_H) \tag{5}$$

In the present work α is taken to depend linearly on the hydrostatic pressure as shown in Fig. 1. The initial distension ratio for the virgin material is α_{00}. For moderate compressions in which the pressure remains less than a critical pressure P_{0e}, the material behaves reversibly, i.e., upon release it will recover its initial distension. In this region

$$\alpha = \alpha_{00} + \alpha_{01} P \qquad P \leq P_{0e} \tag{6}$$

If the pressure P_{0e} is exceeded, irreversible compaction of the material will occur and so long as the material continues to crush

$$\alpha = \alpha_0' + \alpha_1' P \tag{7}$$

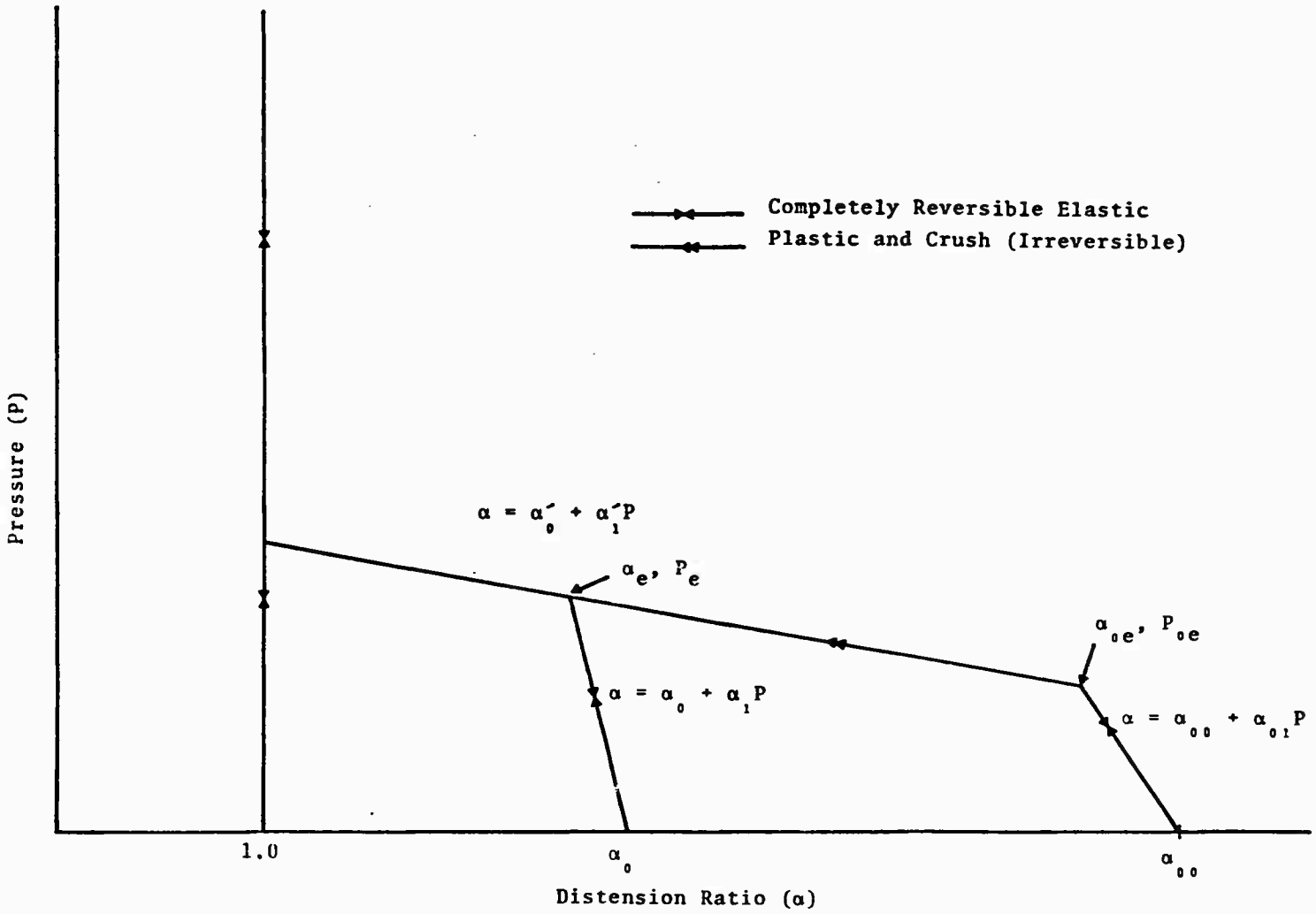

Fig. 1--Pressure vs distension ratio for a generalized porous material.

until all the voids are collapsed at which time $\alpha = 1.0$. Once α attains a value of unity it remains at that value thereafter. If during the crushup process the material is unloaded from some partially compacted state (α_e, P_e) the unloading will occur along a curve such that

$$\alpha = \alpha_0 + \alpha_1 P \tag{8}$$

This α-P curve is reversible in that any reloading of the material will occur along this curve until the state (α_e, P_e) is once again reached. Upon reaching (α_e, P_e) subsequent loading occurs along the irreversible curve, given by Eq. (7). Thus, for a material which has been partially compacted and then unloaded, the pressure P_e becomes the new reversible limit just at P_{0e} was the reversible limit in the virgin material. The reversible and irreversible branches of the α-P curves are denoted by arrowheads in Fig. 1.

The degree of irreversible compaction at any point in the crushup process is accounted for by a progress parameter ϕ. This parameter varies from one to zero as the material passes from the porous state $\alpha = \alpha_{0e}$, where irreversible crushup begins, to the state $\alpha = 1$ where compaction is complete.

$$\phi = \frac{\alpha(\phi) - 1}{\alpha_{0e} - 1} \tag{9}$$

For example, if $\alpha_{0e} = 2.0$, and at some partially crushed state $\alpha = 1.5$, then $\phi = 0.5$ denoting that the material is halfway crushed. The coefficients α_0 and α_1 in Eq. (8) for the reversible loading-unloading path from a partially compacted state are computed from the coefficients α_{00} and α_{01} in Eq. (6) for the initial reversible path and from the

progress parameter ϕ. These coefficients are given by

$$\alpha_0 = (\alpha_{00} - 1)\phi + 1$$
$$\alpha_1 = \alpha_{01}(P_{0e}/P(\phi)) \tag{10}$$

Thus if only a small amount of permanent crushing has occured, i.e., (α_e, P_e) is very near $\alpha_{0e}, P_{0e})$, the loading-unloading α-P curve will be very much like that of the virgin material, hwereas if compaction is almost complete it will be very nearly the vertical line $\alpha = 1$. The progress parameter, ϕ, varies along the irreversible crush curve and remains constant on the reversible curves. The branches of the hydrostatic curve in the P-V plane corresponding to the branches of the α-P curve are shown in Fig. 2. P_{cr} is the pressure at which α reaches unity.

2.2 MATERIAL STRENGTH

In addition to the hydrostatic pressure, which is computed from the equation of state model just described, rigidity and shear yielding affect wave propagation in the porous material. The principal stresses, σ_i, principal stress deviators, S_i, and the hydrostatic pressure are related by

$$\sigma_i = -p + S_i, \quad i = 1, 2, 3 \tag{11}$$

In the region where the material behaves linearly elastic

$$\dot{S}_i = 2\mu\left(\dot{\varepsilon}_i - \frac{1}{3}\frac{\dot{V}}{V}\right) \tag{12}$$

where the dots denote time derivates, μ is the shear modulus, and ε_i is a principal strain. In the porous EOS model provision is made to allow the shear modulus to vary as the material is being crushed. The effective shear modulus μ_e at any point during crushup is

$$\mu_e = \phi\mu_P + (1 - \phi)\,\mu_s \tag{13}$$

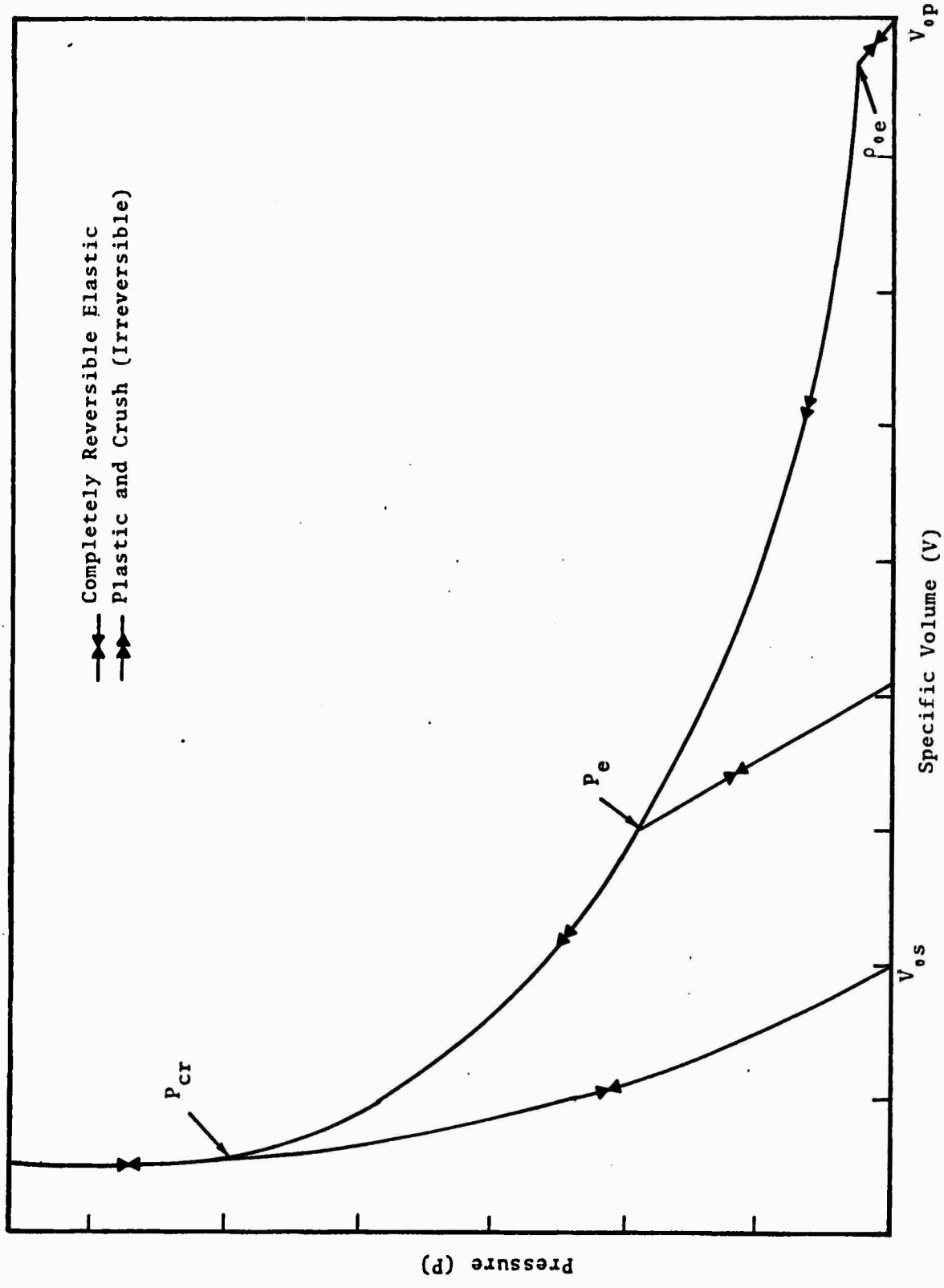

Fig. 2--Pressure vs volume for a generalized porous material.

where μ_p and μ_s are respectively the shear modulii of the porous and solid materials and ϕ is the crushup progress parameter discussed earlier.

The stress deviators are limited by the von Mises yield condition

$$S_1^2 + S_2^2 + S_3^2 \leq \frac{2}{3} Y^2 \tag{14}$$

where Y is a yield strength which may depend upon the hydrostatic pressure. In the present work its dependence upon pressure appears only through the crushup progress parameter. As with the shear modulus, the yield strength Y in the partially compacted region is given by

$$Y = \phi\, Y_{0p} + (1 - \phi)\, Y_{0s} \tag{15}$$

where Y_{0p} and Y_{0s} are respectively constant values of the yield strength of the virgin porous and of the completely compacted material. No pressure enhancement of the yield strength of the compacted rock is considered.

2.3 METHOD OF COMPUTATION

The spherical wave propagation problems in porous and compacted dry tuff were solved using a one-dimensional Lagrangian elastic-plastic computer code called WORKHORSE.[4] This code solves the equations of conservation of mass, momentum and energy using the artificial viscosity technique to smooth shocks. The problem consists of a sphere of tuff which is initially 35 cm in radius and has a 5-cm spherical cavity in the center. Ten problems were run in which an exponentially decaying normal stress pulse of the form

$$\sigma(r_c, t) = 35e^{-t/10} \text{ kbar} \quad (t \text{ in } \mu\text{sec}) \tag{16}$$

was applied to the interior of the cavity. Two problems were run in which a square pulse 35 kbar for 10 μsec was applied to the interior of the cavity. The response of the material as a function of time was computed at stations which were initially 7.5, 10, 12.5, 25, and 30 cm from the center of the sphere. For computational purposes the entire 35-cm radius sphere is divided into 200 zones with the central cavity as zone one. The remaining 199 zones are chosen such that the mass of each zone increases by a factor of 1.02, i.e., $M_{j+1}/M_j = 1.02$. Once the zone size is established the time step in the calculation is controlled by the Courant condition which depends upon the zone size, the sound speed, and the artificial viscosity parameters.

At each cycle in the calculation, values of the hydrostatic pressure, stress deviators, displacement, velocity and the time are printed for the zones being monitored. The stress field results are put on tapes from which plots are obtained for the hydrostatic pressure, radial and tangential stresses as functions of time for the monitored zones.

The values of the equation of state parameters used in the calculations and the results of the calculations are summarized in the next section.

3. SPHERICAL WAVE PROPAGATION IN TUFF

In all of the spherical problems run in this study, the Hugoniot curve $P_H(V)$ of the solid compacted material was taken to be

$$P_H(\eta) = A\eta + B\eta^2 \qquad \eta = \frac{\rho}{\rho_0} - 1$$

where $A = 245.7$ kbar and $B = 298.7$ kbar. Although void-free dry tuff does not occur naturally, this estimate for the pressure-volume relationship was made by Hastings[5] based on the constituents of tuff. The solid density at zero pressure is 2.4 g/cm^3. Also throughout all calculations, the value of Gruneisen's ratio G was taken to be 0.33.

The effect on wave propagation of changes in the following parameters was investigated:

1. P_{cr}, the hydrostatic pressure at which all voids are compacted
2. Y, the yield strength in the von Mises yield condition
3. μ, the shear modulus
4. α_{00}, the initial porosity
5. The effect of fracture due to hoop tensile stress
6. Variation of the elastic α's in the α-P model.

The values of the parameters used in each of the twelve computer runs are presented in Table I. In all except two cases the stress applied to the interior of the cavity was the exponential decay form given in Eq. (16). The two cases in which the square pulse was applied are indicated in Table I.

TABLE I

PARAMETERS USED IN SPHERICAL CALCULATIONS

Run	α_{00}	μ (kbar)	Y (kbar)	P_{cr} (kbar)	Comments
OD	1.0	223	1.0	-	
5A	1.0	223	10.0	-	
6A	1.0	223	10.0	-	Identical to run 5A except that σ_θ set equal to zero to simulate fracture after attaining a value of 1 kbar in tension
8B	1.0	45	10.0	-	
9A	1.0	223	1.0	-	Identical to run OD except square pulse 35 kbar for 10 μsec applied to cavity interior surface
1C	1.05	45-223	0.1-1.0	20	P_{0e} = .01 kbar, α_e = 1.04999, α_1 = -10^{-12}, α_0' = 1.050015, α_1' = -2.5×10^{-12}
2A	1.05	45-223	0.1-1.0	40	Same α's as 1C, P_{0e} same as in 1C
4A	1.05	45-223	1.0-10.0	20	Same α's as 1C, P_{0e} same as in 1C
7A	1.05	45-223	0.1-1.0	20	Identical to run 1C except $\alpha_{00} = \alpha_0'$ and $\alpha_{01} = \alpha_1'$
10A	1.05	45-223	0.1-1.0	20	Identical to run 1C except square pulse 35 kbar for 10 μsec applied to interior cavity surface
3C	1.25	45-223	0.1-1.0	20	P_{0e} = .01 kbar, α_e = 1.24999, α_1 = -10^{-12}, α_0' = 1.250015, α_1' = -1.251×10^{-11}
11A	1.25	45-223	0.1-1.0	20	Identical to run 3C except $\alpha_{00} = \alpha_0'$ and $\alpha_{01} = \alpha_1'$

3.1 PEAK STRESS

Peak radial stress, σ_r, peak tangential stress, σ_θ, and peak hydrostatic pressure, P, as functions of radius, are given in Table II. Peak tensile stresses and precursor amplitudes are also indicated in some of the runs in Table II. Curves of the attenuation of peak radial stress as a function of radius are plotted for selected runs in Fig. 3. All runs were not plotted as the results of several were quite similar. However, the curves shown in Fig. 3 do span all of the radial stress attenuation curves for the ten runs in which the exponential decay stress pulse was applied to the cavity. In all cases the attenuation was lowest in the compacted material, greater in the 5-percent porous material and greatest in the 20-percent porous material. This variation of the porosity from zero to 20 percent, leaving the other parameters constant (compare runs 0D, 1C, and 3C), gave greater peak stress attenuation than variation of the other material parameters over a range which might reasonably be representative of dry tuff.

Five runs were made on compacted material to assess the effect on attenuation of parameters other than porosity. The material in run 0D (μ = 223 kbar, Y = 1.0 kbar) may be considered as a standard and the radial stress attenuation curve for this material is shown in Fig. 3. The material in run 5A was the same as 0D except that Y was increased to 10 kbar. The rate of attenuation of peak stress, not shown in Fig. 3, was slightly greater than in run 0D (see Table II. However, greater hoop tensile stresses and larger precursors occurred. Run 6A was identical to 5A except that the hoop stress was set equal to zero after attaining a value of 1 kbar in tension. The simulated fracture, occurring in tension, produced no effect on the attenuation of peak stress, but did naturally limit the tension occurring after the peak, and, as we shall see, changed the displacement and velocity

TABLE II

PEAK STRESS AS A FUNCTION OF RADIUS

Run \ r	7.5 cm			10 cm			12.5 cm			25 cm			30 cm		
	σ_r	σ_θ	P	σ_r	σ_θ	P	σ_r	σ_θ	P	σ_r	σ_θ	P	σ_r	σ_θ	P
OD	19.5	18.6 -.5	18.5	13.8	12.7 -.4	13.0	10.6	9.5 -.3	9.9	3.75	2.75	3.1	--	--	--
5A	18.2	8.4 -2.4	11.7 (4.4)	11.7 (8.0)	1.75 -2.0 (.95)	5.3 (3.3)	8.2	.8 -2.1	2.7	3.5 -.7	.4 -.52	1.35	2.8	.34 -.32	--
6A	18.3 (11)	8.4 -1.0	11.7 (4.4)	11.7	1.75 -1.0 (.95)	5.3 (3.3)	8.2	.8 -1.0	2.65	3.5 -1.3	.4 -.6 .65*	1.35	2.8 -1.5	.34 -.36 .75*	1.1
8B	21	15.6 -2.5	16.7	14.6	10.2 -1.3	11.6	11.1	7.7 -.8	8.8	4.6	3.2 -.2	3.7	3.6	2.5 -.1	2.86
9A	25.6	24.5 -.5	25	19.6 (1)	18.6 -.5	19 (.4)	15.7 (.75)	14.7 -.4	15.0 (.3)	5.5 (.4)	4.5	4.85 (.15)	3.25 (5) -.7	2.25	2.6 (.14)
1C	16.5	15.7 -.2	15.7	10.2	9.8	9.9	7.1	6.8	6.9	1.9	1.73	1.8	1.46	1.27	1.34
2A	17.6	17.1	17.2	11.7	11.4	11.5	8.2	7.95	8.05	2.35	2.17	2.23	1.5	1.37	1.4
4A	16	9.7 -2.0	11.8	9.6	5.6 -1.0	6.9	6.3	3.4 -.5	4.37	1.24	.65	.84	.44	.25	.31
7A	16.5	15.6 -.2	15.8	10.5	9.8	10	7.2	6.8	6.9	1.7	1.52 (.1)	1.62 (.15)	1.07	.92 .04	.97 (.04)
10A	25.6	24.5	25	19	18.2 -.2	18.5	11.7	11.1	11.5	1.27	1.12	1.17	.8	.68	.72
3C	13	12.5	12.6	7.1	6.6	6.8	4.2	3.95	4.0	--	--	--	--	--	--
11A	13.6	13	13.2	7.4 (.2)	7.0	7.2 (.1)	4.6 (.1)	4.2 (.05)	4.3 (.1)	0.8 (.06)	.66 (.02)	0.7 (.04)	--	--	--

NEGATIVE VALUES DENOTE PEAK TENSILE STRESS

NUMBERS IN PARENTHESIS DENOTE PRECURSOR AMPLITUDE

*SECOND MAXIMUM OCCURRING AFTER TENSION

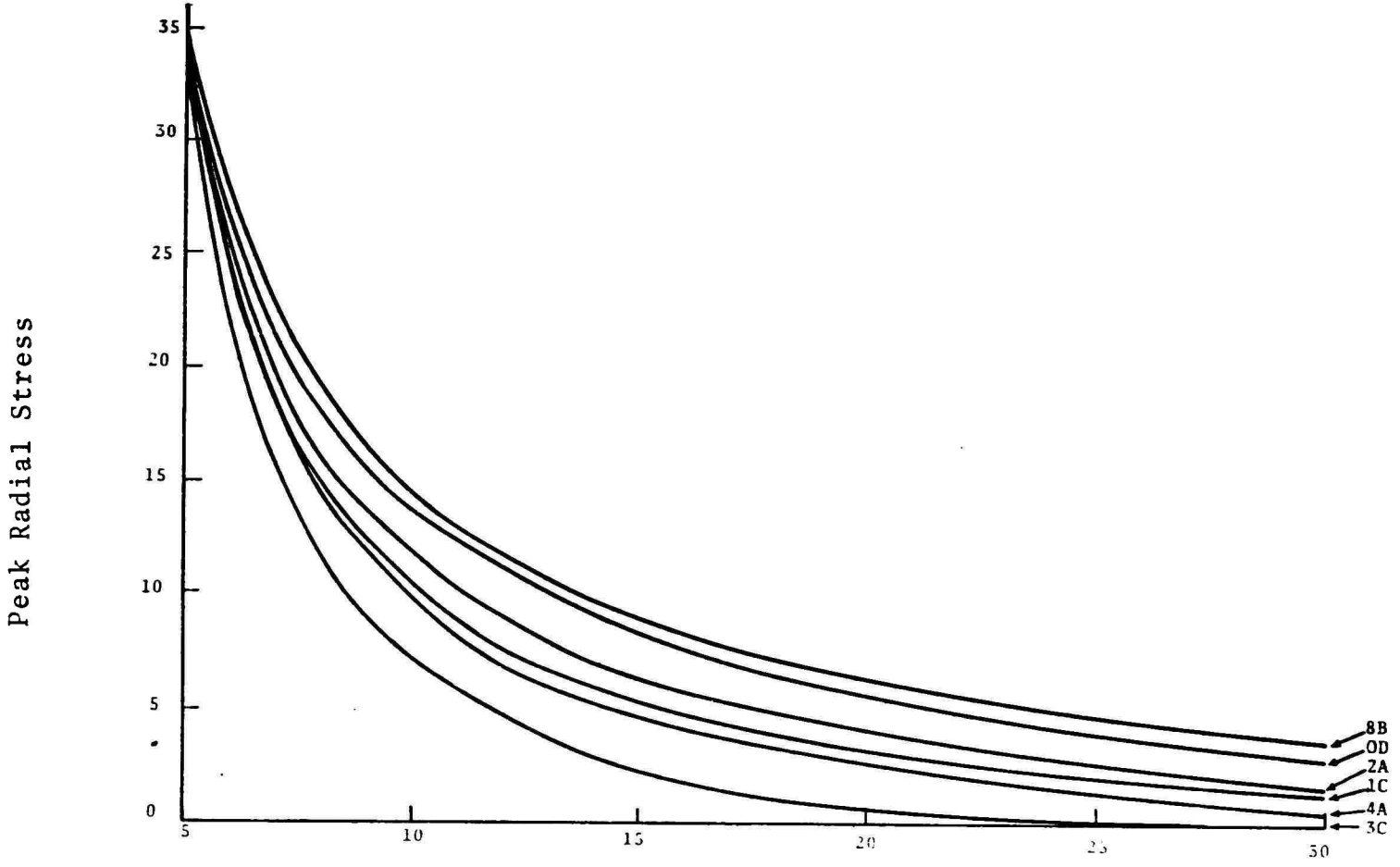

Fig. 3--Attenuation of peak radial stress.

field from that when no fracture occurred. In run 8B the fracture condition was removed, the yield Y was kept at 10 kbar and the shear modulus μ was reduced to 45 kbar. As can be seen in Fig. 3 decreasing the shear modulus by a factor of five reduces the attenuation enough to more than compensate for the increase in attenuation produced by increasing the yield strength by a factor of ten, e.g., run 0D to 5A. In problem 9A in which the square pulse was applied to the cavity interior, the material parameters were all the same as those in problem 0D. The attenuation of the peak stress in problem 9A was much slower than in 0D as can be seen from Table II. Radial stress-time profiles for problem 0D are presented in Fig. 4.

Five problems (four with exponential decay pulse and one with the square pulse applied to the cavity interior) were run for five percent (α_{00} = 1.05) porosity material. The material in the run 1C (μ = 45-223 kbar, Y = 0.1-1.0 kbar, P_{cr} = 20 kbar) may be considered as a standard. The attenuation of peak radial stress for this run is shown in Fig. 3. Problem 2A was run with the same parameters as 1C except that the crushup pressure, P_{cr}, was increased by a factor of two to 40 kbar. From Table I and Fig. 3 it is apparent that increasing the crushup pressure reduces the rate of peak stress attenuation. In run 4A all was the same as in run 1C except that the range of the yield strength Y was increased by an order of magnitude. Here, as in the compacted material, the attenuation rate of peak stress was increased. In run 7A all parameters were the same as standard run 1C except that the α coefficients for the elastic portion of the hydrostat were set equal to those of the irreversible portion. No significant change in peak stress attenuation was observed from that of run 1C. This is apparently due to the fact that at five percent porosity, the elastic portion of the hydrostat and

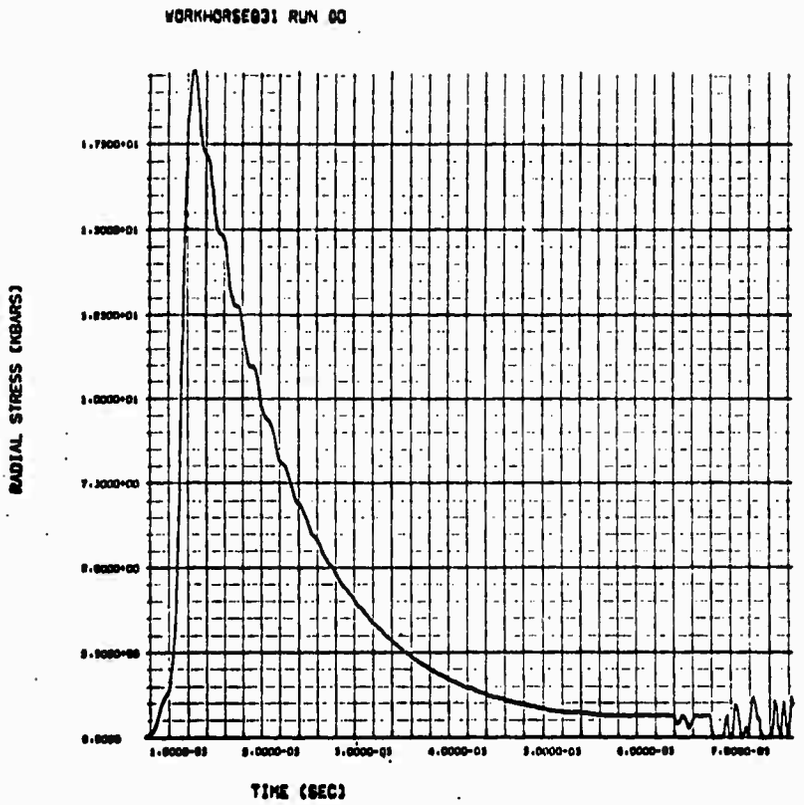

Fig. 4(a)--Station 17, 7.5 cm.

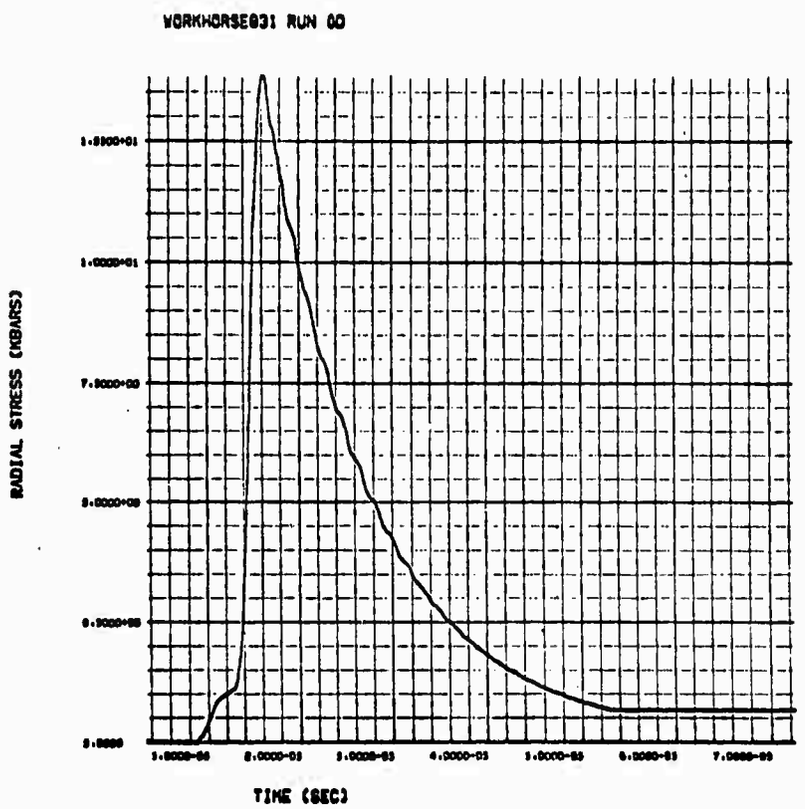

Fig. 4(b)--Station 38, 10 cm.

Fig. 4--Radial stress-time profiles for Run OD.

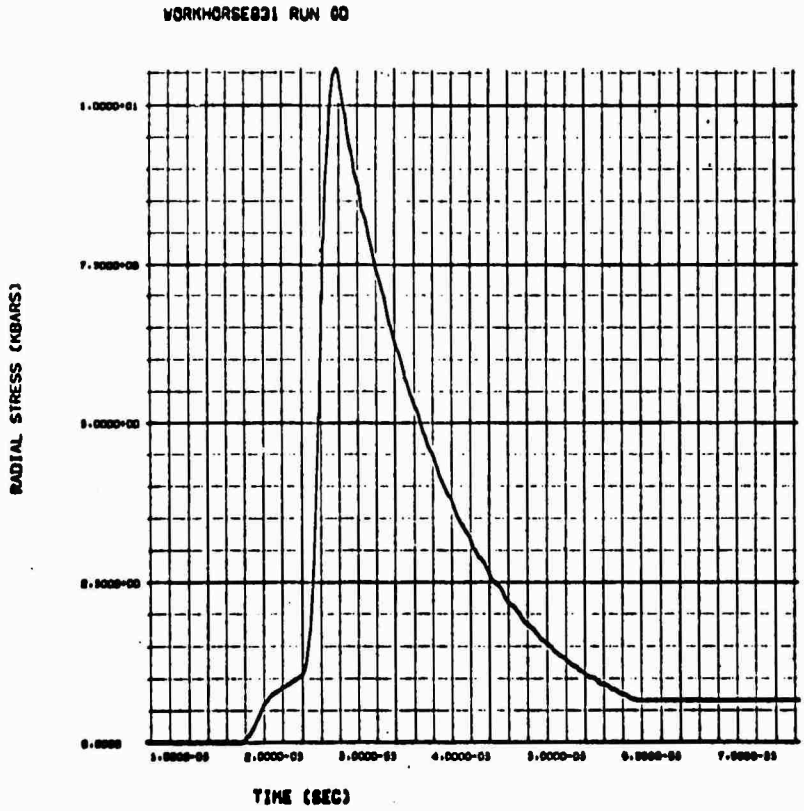

Fig. 4(c)--Station 60, 12.5 cm.

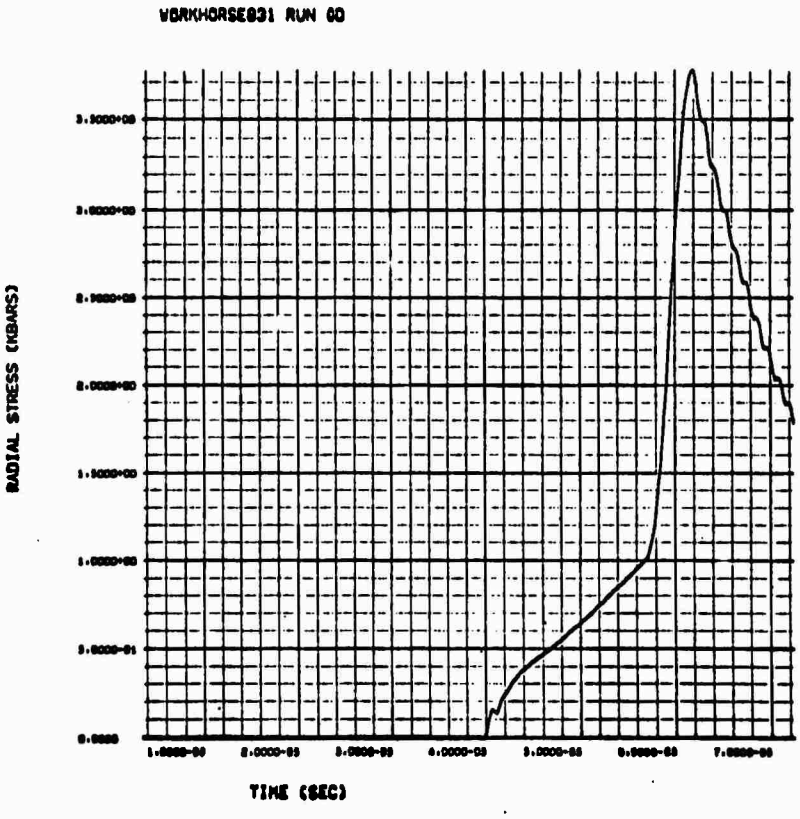

Fig. 4(d)--Station 151, 25 cm.

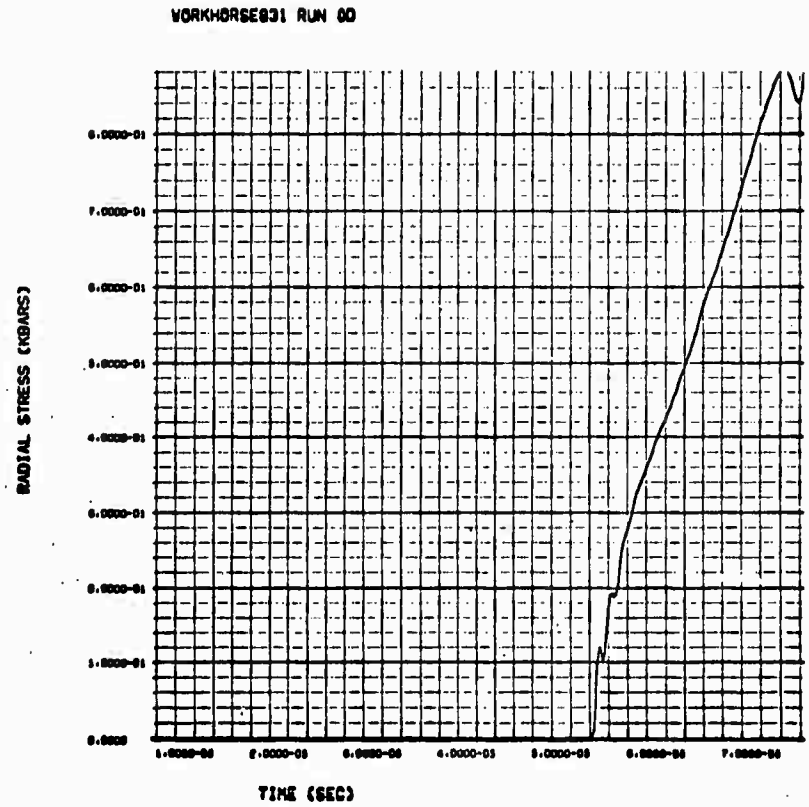

Fig. 4(e)--Station 178, 30 cm.

the crushup portion in 1C had very nearly the same slope so that varying the α coefficients as was done in 7A had little effect on the release curves. Radial stress-time profiles at the monitored stations for run 1C are presented in Fig. 5. For comparison of the effect of the shape of the pulse applied to the cavity interior, radial stress-time profiles for run 10A, which is identical to 1C except that a square pulse is applied, are presented in Fig. 6.

In run 3C, the initial porosity is increased to $\alpha_{00} = 1.25$. This run exhibited the greatest attenuation of peak stress with distance as can be seen from the radial stress attenuation curve in Fig. 3 and the tabulated values in Table II. Radial stress-time profiles for run 3C are presented in Fig. 7. Run 11A was the same as 3C except that the α coefficients in the elastic portion of the hydrostat were set equal to those of the crushup portion. In this case the attenuation of peak stress was slightly less than that of 3C. This result is what one would anticipate since the release curves are more parallel to the crush curve in run 11A than in 3C. Having the release curves more parallel to the crush curves simulates a more reversible release, i.e., more opening up of pores on release, thereby producing less dissipation of energy and less attenuation. In the five-percent porosity cases, runs 1C and 7A, this effect was also anticipated but, as mentioned earlier, the difference in the release curves in the two cases apparently was not significant for those two cases.

3.2 ARRIVAL TIMES AND PULSE WIDTHS

Arrival times and pulse widths at 1/2 peak and 1/4 peak stresses are presented in Table III. Some of the time of arrival (TOA) columns contain two, three or four entries. The first entry always refers to the time of first motion. The last entry is always the arrival time of the peak. In some cases

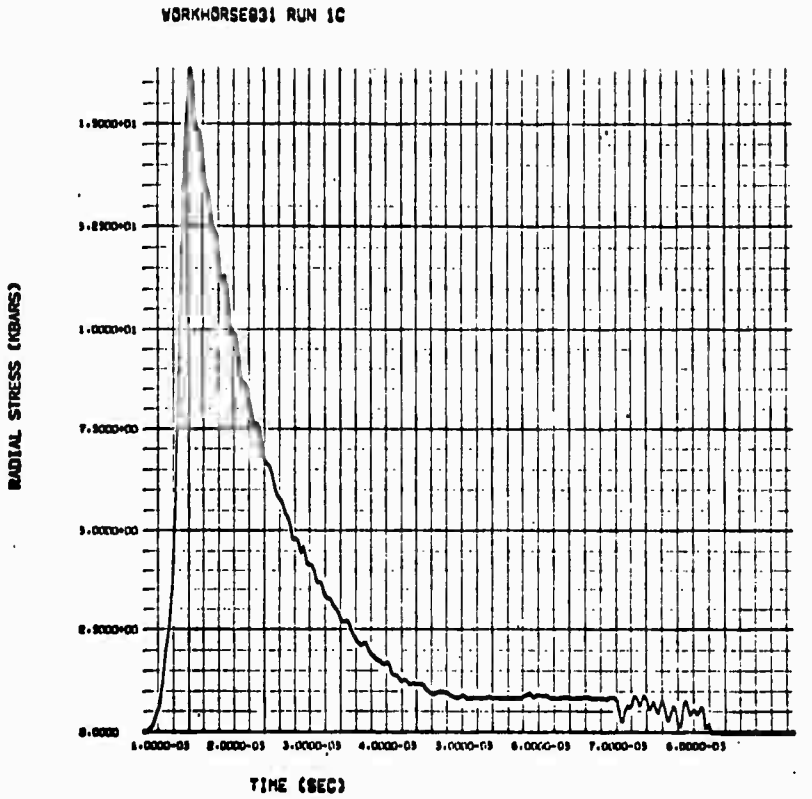

Fig. 5(a)--Station 17, 7.5 cm.

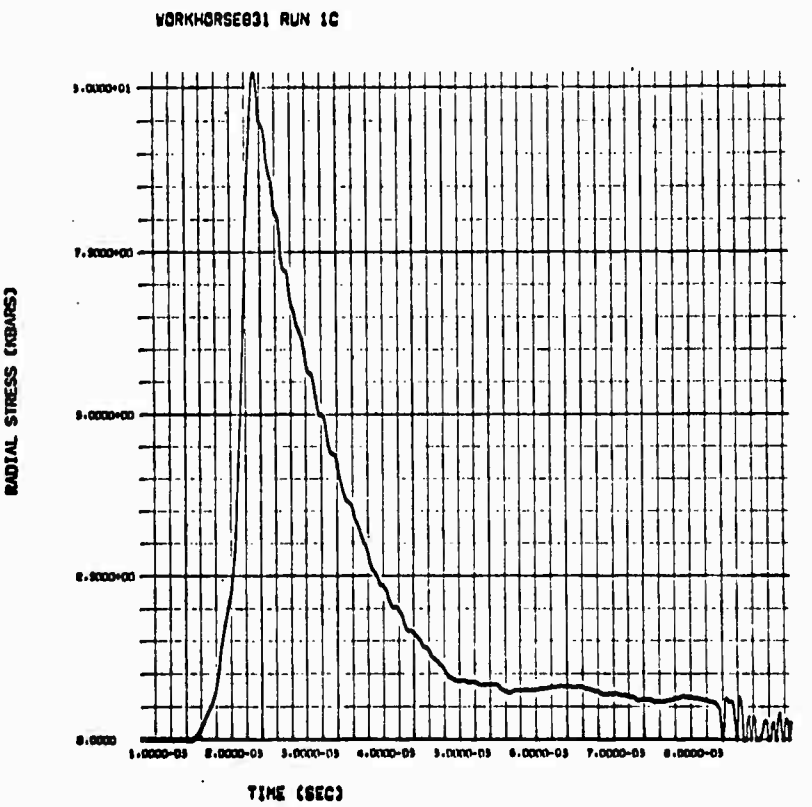

Fig. 5(b)--Station 60, 10 cm.

Fig. 5--Radial stress-time profiles for Run 1C.

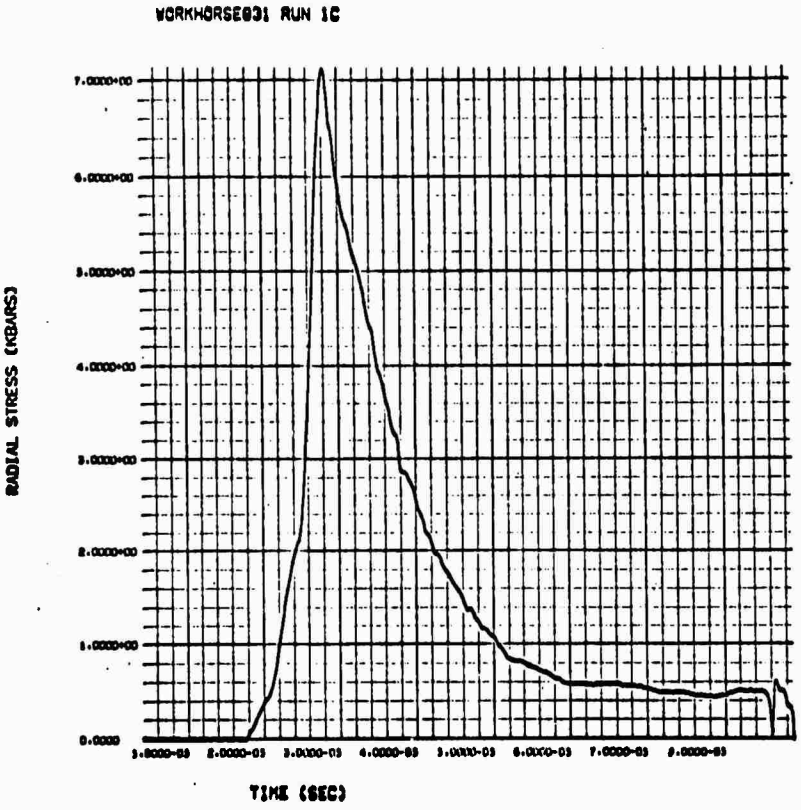

Fig. 5(c)--Station 151, 12.5 cm.

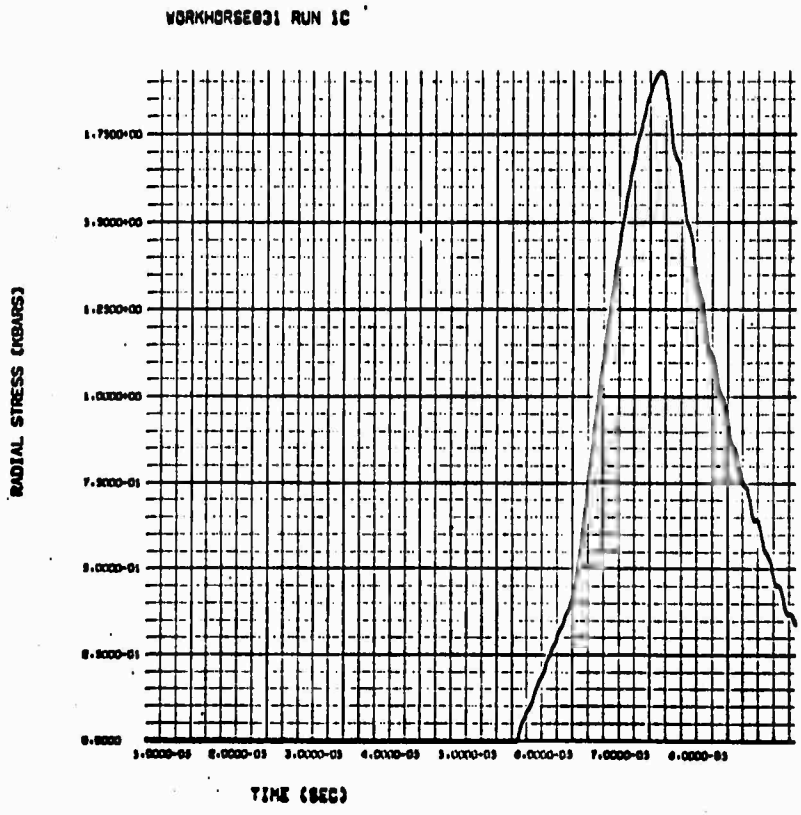

Fig. 5(d)--Station 151, 25 cm.

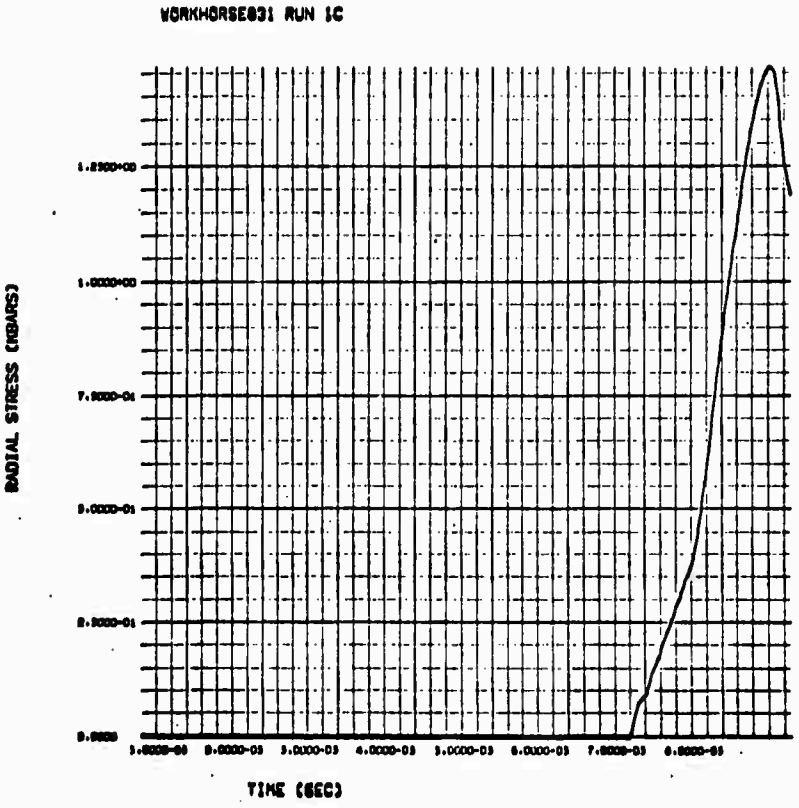

Fig. 5 (e)--Station 178, 30 cm.

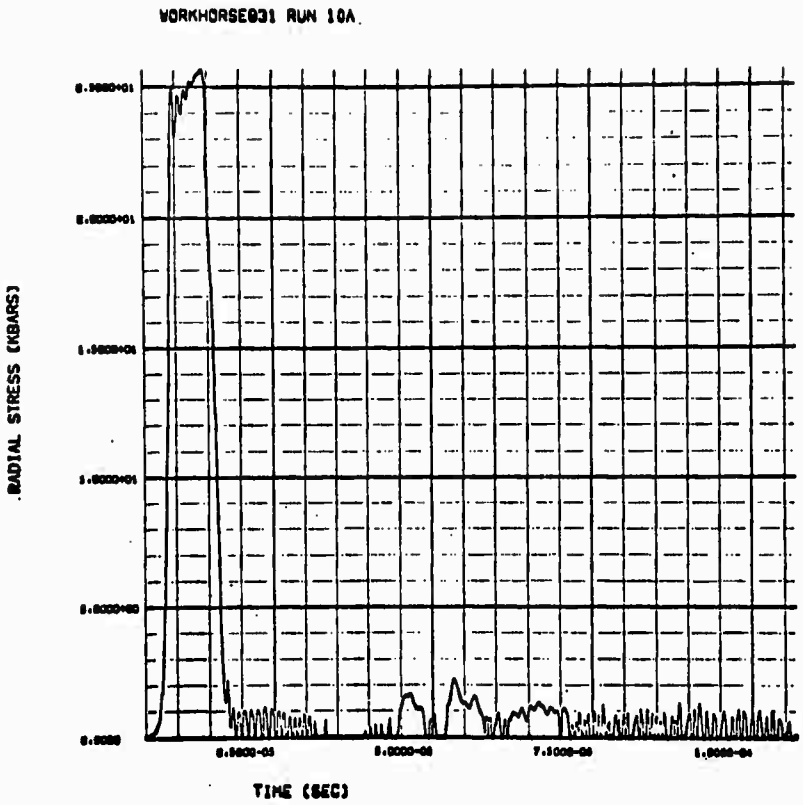

Fig. 6(a)--Station 17, 7.5 cm.

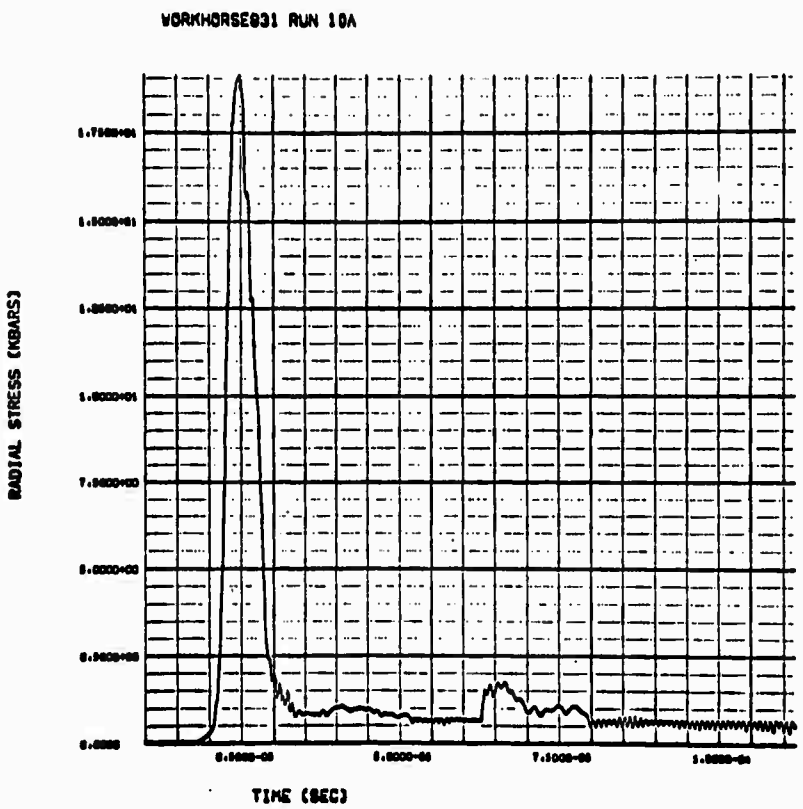

Fig. 6(b)--Station 38, 10 cm.

Fig. 6--Radial stress-time profiles for Run 10A.

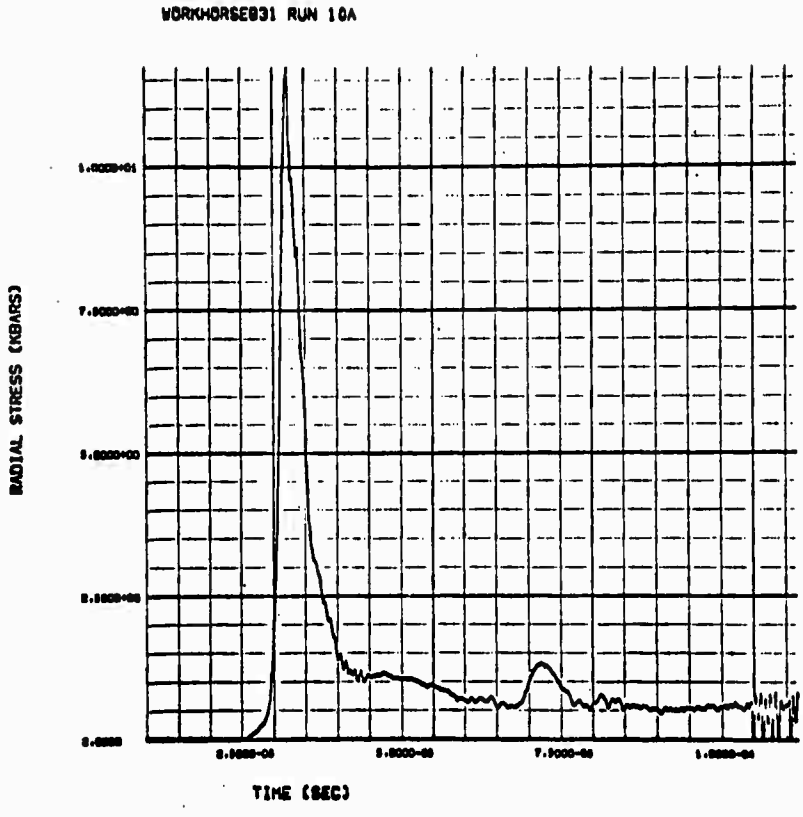

Fig. 6(c)--Station 60, 12.5 cm.

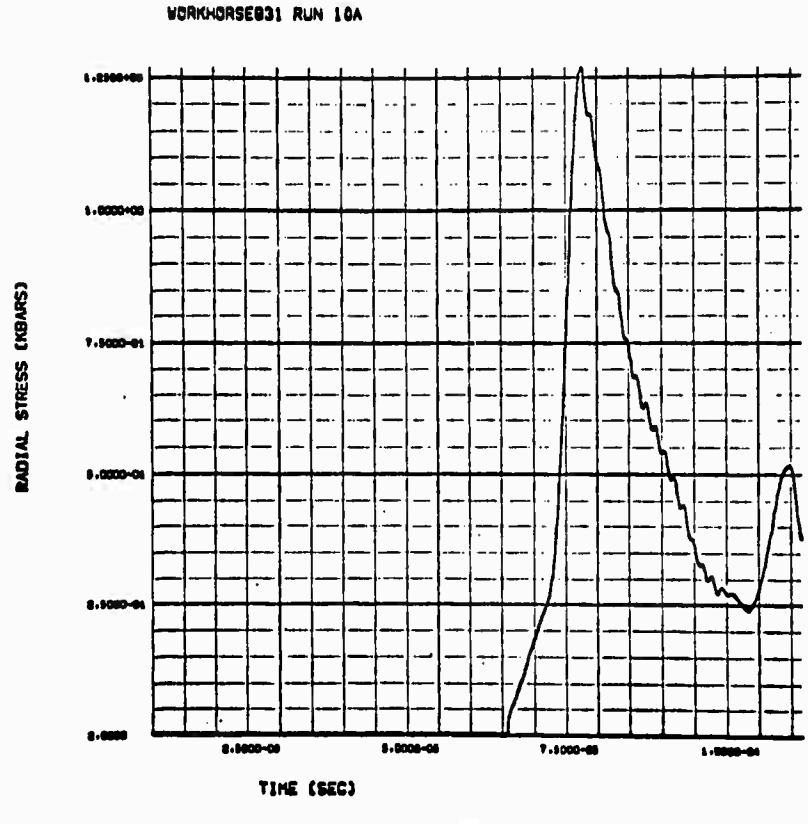

Fig. 6(d)--Station 151, 25 cm.

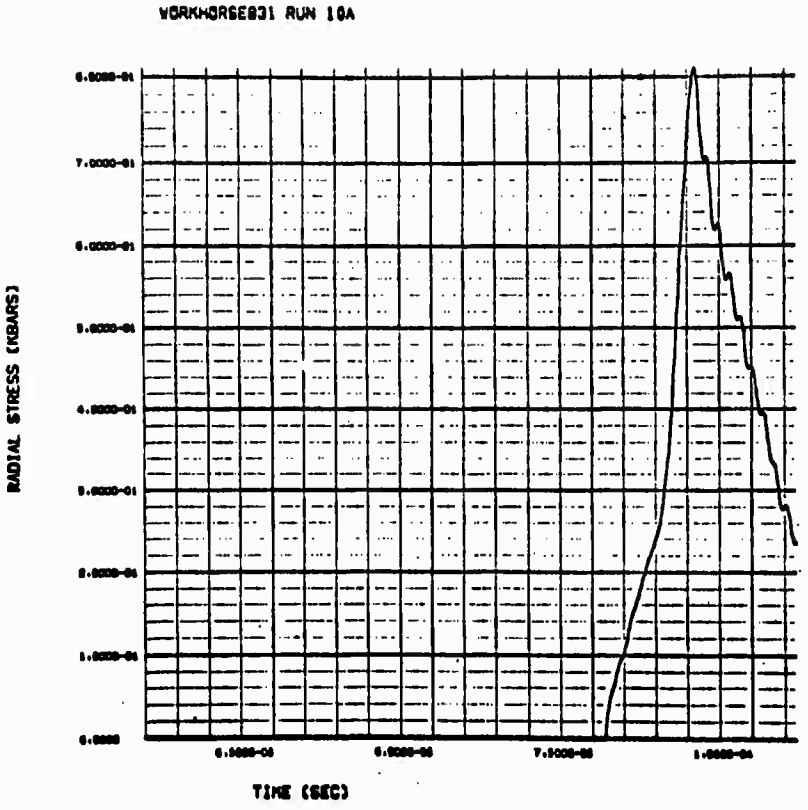

Fig. 6 (e)--Station 178, 30 cm.

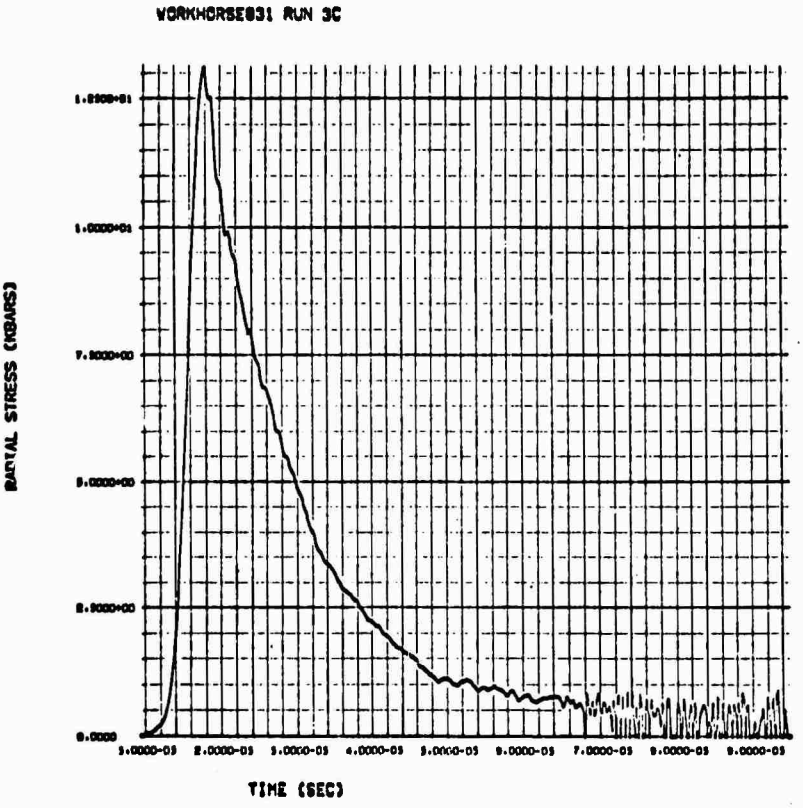

Fig. 7(a)--Station 17, 7.5 cm.

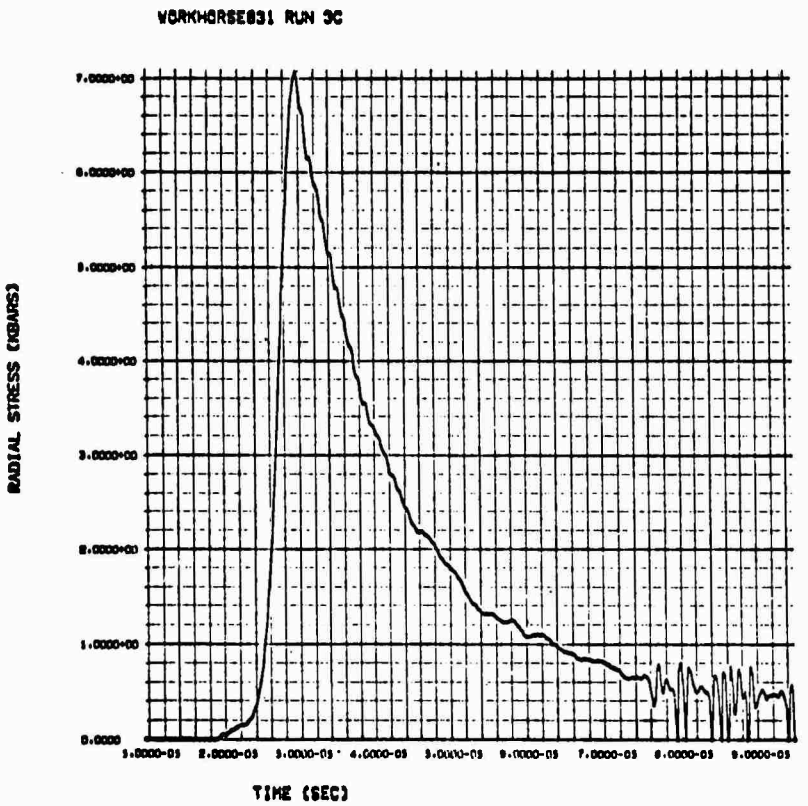

Fig. 7(b)--Station 38, 10 cm.

Fig. 7--Radial stress-time profiles for Run 3C.

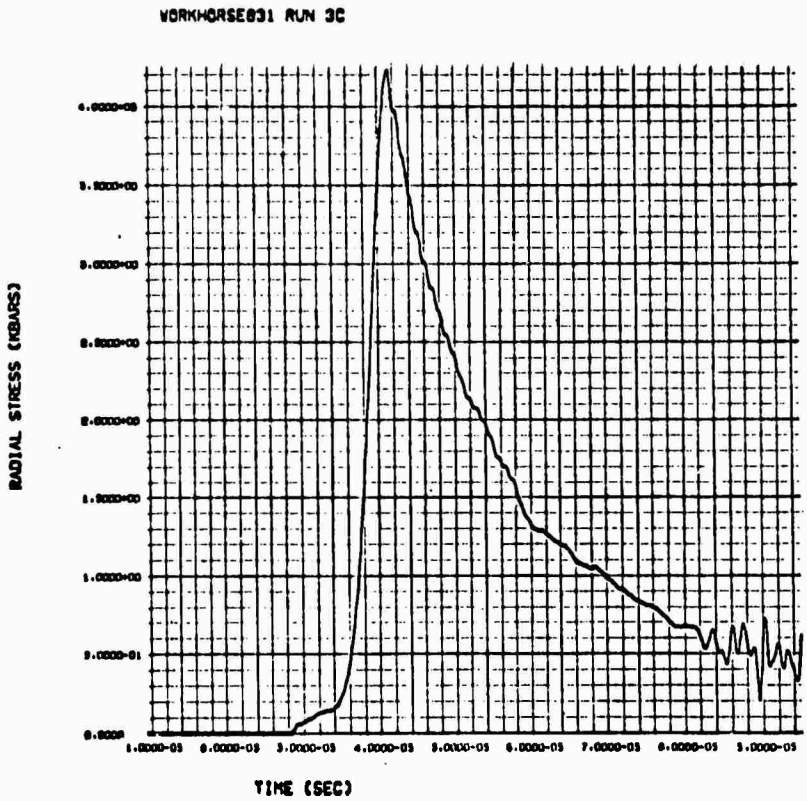

Fig. 7(c)--Station 60, 12.5 cm.

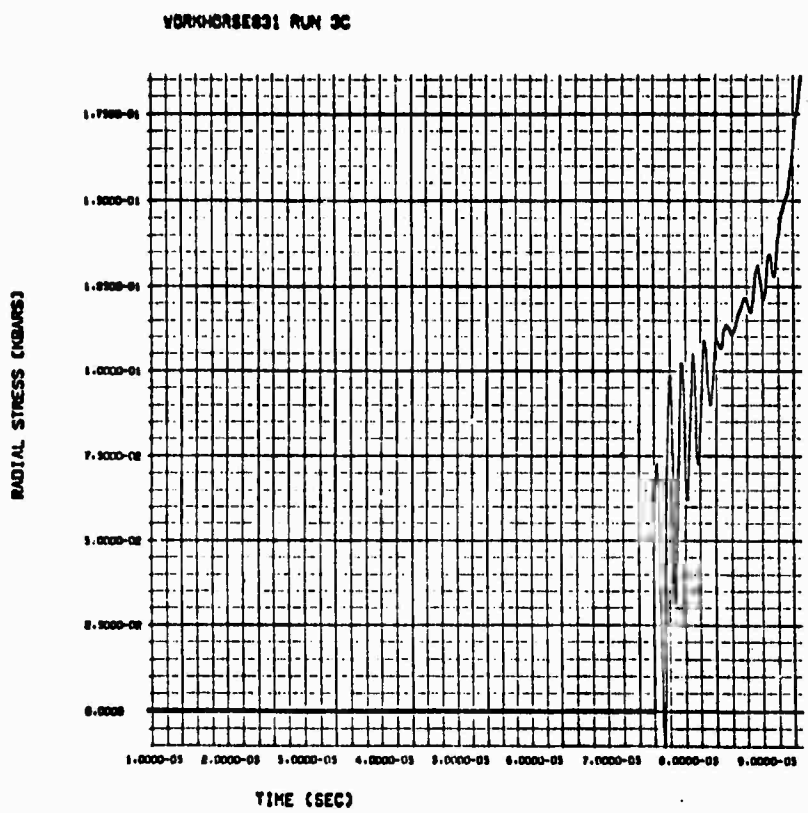

Fig. 7(d)--Station 151, 25 cm.

only a ramped precursor was evident and in those cases three entries appear, the middle one being the arrival time of the bottom of the plastic wave. In other cases a more well-defined precursor was formed and in those cases, denoted by four entries, the second entry is the arrival time of the precursor peak and the arrival time of the bottom of the plastic wave. As can be seen from the entries in Table III, the arrival times for the waves at the different stations are generally lowest in the compacted material, greater in the five-percent and greatest in the 20-percent porous material. The pulse widths at 1/2 peak and 1/4 peak show remarkably little variation from station to station in a given run in many of the runs although the peak stresses, as we have seen, have greatly attenuated.

3.3 DISPLACEMENT AND VELOCITY

The position and velocity of the monitored grid cells at about 75 μsec after application of the pulse to the cavity interior are presented in Table IV. The problems on the compacted material generally ran in fewer cycles corresponding to a shorter total wave propagation time than the problems on the porous material. Total times ran from about 75 μsec to over 100 μsec. Therefore, in order to compare positions and velocities at the same time, 75 μsec was chosen. The particles initially located at 7.5, 10, and 12.5 cm from the cavity center generally show increasing displacement and velocity with increasing porosity. In the compacted material runs 5A and 6A,where the yield strength was increased to 10 kbar, show an effect of pulling back toward the center of the problem. In fact, in run 6A, which differs from 5A only in that the fracture condition on the hoop stress was introduced, all particles have a negative velocity, i.e., toward the center, and the particles at the 7.5, 10, and 12.5 cm stations

TABLE III

ARRIVAL TIMES AND PULSE WIDTHS AS FUNCTIONS OF RADIUS

Run \ r	7.5 cm		10 cm		12.5 cm		25 cm		30 cm	
	TOA*	Width ½, ¼ Peak	TOA	Width ½, ¼ Peak	TOA	Width ½, ¼ Peak	TOA	Width ½, ¼ Peak	TOA	Width ½, ¼ Peak
OD	4, 8.5	8.5, 15	9, 13, 16	9, 18	14, 20, 24	10, 19	40, 57, 62	12, --	50.5, 70, --	--
5A	4, 7, 9	10, 16	9, 12, 15, 16.5	12, 18	13.5, 20	12, 18	39, 46	10, 24	49, 58	9, 13
6A	4, 7, 9	10, 18	9, 12, 15, 16.5	12, 18	13.5, 20	13, 20	39, 46	11, 26	49, 58	10, 19
8B	5, 8	7, 12	11, 14.5	7, 13	17,21	17, 12	50, 56.5	8, 13	64, 71	8, 13
9A	4, 8	9, 10	9, 11 13, 20	8, 10	14, 17 20, 27	8, 10	40, 43, 57, 61	8, 20	51, 53 72, 76	10, 26
1C	5, 10	9, 18	11, 19	10, 19	18, 28	11, 20	53, 71	17, 26	68, 86	--
2A	5, 9.5	9, 16	12, 18	10, 16.5	19, 26	10, 16.5	56.5, 68	11, 18	72, 84	
4A	5, 9.5	8, 15	12, 18	7, 11	19.5, 25.5	4, 4.5	57, 62.5	1, 2	73, 77	1, 2
7A	5, 10	9, 18	13, 19	11, 18	21, 28	10, 20	62, 67, 73	12, 23	78, 86, 93	13, 20
10A	5, 10	7, 9	13, 20	6, 7	21, 23, 27	4, 7	61, 62, 67, 73	12, 24	77, 78, 86, 92	14, 25
3C	6, 14	5.5, 10	15, 25	6, 26	24, 37	14, 31	72, --	--	--	--
11A	5, 13	10, 19	16, 20, 26	12, 24	26, 27, 31, 38	18; 34	75, 77, 85, 98	--, --	97, --, --	--

ALL TIMES IN μSEC

*TWO ENTRIES: TOA FIRST MOTION, TOA PEAK (PRECURSOR NOT WELL DEFINED OR ABSENT)
THREE ENTRIES: TOA FIRST MOTION, TOA BOTTOM PLASTIC WAVE, TOA PEAK (RAMPED PRECURSOR)
FOUR ENTRIES: TOA FIRST MOTION, TOA TOP PRECURSOR, TOA BOTTOM PLASTIC WAVE, TOA PEAK

TABLE IV

POSITION AND VELOCITY AT t ∿ 75 μSEC

Run \ r	7.5 cm		10 cm		12.5 cm		25 cm		30 cm	
	R	V	R	V	R	V	R	V	R	V
OD	8.20	4.62	10.4	3.10	12.78	2.25	25	2.42	30	1.01
5A	7.55	-1.54	10.0	2.19	12.50	2.30	25	-1.26	30+	1.61
6A	7.42	-4.89	9.95	-2.27	12.4	-2.35	25	-1.5	30+	1.47
8B	7.83	.703	10.2	1.20	12.6	.48	25	.61	30+	2.43
9A	8.39	9.34	10.5	5.61	12.85	3.86	25+	2.90	30	4.03
1C	8.55	9.6	10.6	8.00	12.8	5.09	25	2.41	30	4.77
2A	8.58	12.5	10.6	8.38	12.8	5.26	25	2.35	30	.24
4A	8.13	7.21	10.3	4.11	12.6	2.20	25	2.62	30	.37
7A	8.56	11.2	10.6	7.45	12.8	5.00	25	2.67	-	-
10A	8.70	11.3	10.7	7.65	12.84	5.33	25	1.9	-	-
3C	8.93	14.9	10.7	9.59	12.85	6.85	25	.178	-	-
11A	8.91	13.9	10.7	9.88	12.86	6.99	25	.02	-	-

Position in cm and velocity in 10^3 cm/sec

are nearer the center at 75 μsec than they were initially. In many of the runs very little motion has occurred at the 25 and 30 cm stations at 75 μsec. Although the material has attained a velocity of the order of 10^3 cm/sec, not enough time has elapsed for any significant motion to occur.

4. SUMMARY

Spherical one-dimensional computer code calculations have been performed to evaluate the importance of certain mechanical material property parameters on stress wave propagation in dry porous rocks. The material property parameters were chosen in a range that is representative of Nevada Test Site tuff. It was found that for a given boundary condition the attenuation of peak stress was most sensitive to the initial porosity of the material with the attenuation rate increasing with increasing porosity. In solid material, i.e., material having no initial porosity, the rate of peak stress attenuation increased with increasing shear modulus and with increasing yield strength being most sensitive to the shear modulus. Shock arrival times at various distances from the source generally increased with increasing porosity, thereby implying that average shock velocities decreased with increasing porosity. Particle displacements at a given time and station increased with increasing porosity. In the initially solid material, tensile stresses that occurred increased with increasing yield strength and the material exhibited in some cases negative displacements, i.e., the material initially moved radially outward from the source and then pulled back inward toward the source. This pull-back was increased by subjecting the material to a fracture condition under hoop tensile stress. A slight decrease in peak stress attenuation in porous material was obtained by increasing the value of the hydrostatic pressure at which all voids are collapsed.

The work reported here studied the effects of varying mechanical material property parameters in a dry porous rock. Further parameter studies are needed using different equation-of-state models to evaluate the effects of water in the pores and to evaluate thermodynamic effects. Parameter studies

are also needed on hard rocks such as granite using finite deformation plasticity theory instead of the usual theory of plasticity based on the infinitesimal strain approximation.

REFERENCES

1. Hastings, C. R., and J. M. Walsh, "Stresses and Stress Wave Effects Due to Heating in Porous Materials," Systems, Science and Software Final Report 3SR-60, November 6, 1968.

2. Hastings, C. R., "The S^3 Porous E-O-S Model," Systems, Science and Software Report 3ST-322, April 17, 1970.

3. Herrmann, W., "Constitutive Equation for the Dynamic Compaction of Ductile Porous Materials," J. Appl. Phys. 40, 2490 (1969).

4. Johnson, W. E., "WORKHORSE: A One-Dimensional Lagrangian Elastic-Plastic Code," General Atomic Report GAMD-8053, July 1, 1967.

5. Riney, T. D., S. K. Garg, C. R. Hastings, J. W. Kirsch, and L. W. Morland, "Stress Wave Effects in Inhomogeneous and Porous Earth Materials," Report No. DASA-2498 on Contract DASA 01-69-C-0159, Systems, Science and Software, March 31, 1970.

UNCLASSIFIED

Security Classification

DOCUMENT CONTROL DATA - R & D

(Security classification of title, body of abstract and indexing annotation must be entered when the overall report is classified)

1. ORIGINATING ACTIVITY (Corporate author)
Systems, Science and Software
Post Office Box 1620
La Jolla, California 92037

2a. REPORT SECURITY CLASSIFICATION
Unclassified

2b. GROUP

3. REPORT TITLE
Determination of Test Needs for the PRIME ARGUS Program

4. DESCRIPTIVE NOTES (Type of report and inclusive dates)
Final Report

5. AUTHOR(S) (First name, middle initial, last name)
G. D. Anderson

6. REPORT DATE	7a. TOTAL NO. OF PAGES	7b. NO. OF REFS
December 30, 1970	40	5

8a. CONTRACT OR GRANT NO.	9a. ORIGINATOR'S REPORT NUMBER(S)
DASA 01-70-C-0122	3SR-513
b. PROJECT NO. (ARPA Order No. 1438)	
c. Program Code Number 0F10	9b. OTHER REPORT NO(S) (Any other numbers that may be assigned this report) DASA-2665
d.	

10. DISTRIBUTION STATEMENT

11. SUPPLEMENTARY NOTES

12. SPONSORING MILITARY ACTIVITY
Director
Advanced Research Projects Agency
Washington, D. C. 20305

13. ABSTRACT

A series of spherical one-dimensional computer code calculations was performed to assess the effects of mechanical material property parameters on wave propagation in dry porous and compacted tuff. Peak stress attenuation was found to be most sensitive to initial porosity. In compacted material peak stress attenuation was found to be more sensitive to the shear modulus than to the yield strength. Increasing hoop tensile stresses occurred with increasing yield strength. Introduction of a hoop tensile fracture criterion did not affect peak stress attenuation but did affect the radial displacement. Generally, radial displacements of particles at the same initial radius from the source increased with increasing porosity. Shock wave arrival times at various distances from the source increased with increasing porosity.

DD FORM 1 NOV 65 1473

UNCLASSIFIED

Security Classification

14. KEY WORDS	LINK A		LINK B		LINK C	
	ROLE	WT	ROLE	WT	ROLE	WT
Stress Waves in Geologic Media						
Nevada Test Site Tuff						
Stress Waves in Porous Media						
Effect of Mechanical Properties on Wave Propagation						